

DYNAMIC CHARACTERISTICS OF MAGNETIC COUPLING IN HORIZONTAL AXIS WAVE ENERGY DEVICE

Jian Zhang^{1,2}

YanJun Liu^{1,2,3}

Jingwen Liu^{1,2}

Tongtong He³

Yudong Xie^{1,2}

¹School of Mechanical Engineering, Shandong University, Jinan, Shandong 250061, China,

²Key Laboratory of High Efficiency and Clean Mechanical Manufacture, Ministry of Education

³Institute of Marine Science and Technology, Shandong University, Qingdao, Shandong 266237, China

ABSTRACT

To solve the dynamic response problems of magnetic coupling in the horizontal axis wave energy device, this has researched the dynamic characteristics of magnetic coupling. The fitting formula about torque and angle of the magnetic coupling is obtained through experiments. The mathematical models of the magnetic coupling torque transmission are established. The steady state error of the magnetic coupling and the transfer function of the output angle are obtained. The analytical solution of the step response of the output angle in time domain is derived. The influence of the torsional rigidity, the damping coefficient and the driven rotor's rotational inertia on dynamic characteristics of the magnetic coupling is analyzed. According to the analysis results, the design rules of magnetic coupling are proposed.

Keywords: Wave energy; Magnetic coupling; Dynamic characteristics; Transfer function; Step response; Steady state error

INTRODUCTION

Because of the global energy crisis, many countries are concentrating on developing renewable energy which has great benefits. Wave energy is an important renewable energy and it shows great development values because it is clean, pollution-free, abundant and widespread [1-6]. The wave energy utilization methods include mechanical, pneumatic and hydraulic forms, which are used in different situations accordingly [7-9], and whose service life, working performance and conversion efficiency are affected by various factors [10-12].

The horizontal axis wave energy device is a kind of mechanical utilization, in which wave energy captured by water turbine drives the generator. During the sea trials, the problems such as seal failure and excessive starting torque

of the mechanical drive device were found. In order to solve these problems, the magnetic coupling is applied, which is an isolated transmission and usually used in the situation where strict sealing property is required to achieve complete sealing [13-17].

If the transmission device is rigid, the unstable movements caused by random waves would directly affect the driven rotor [18]. However, the magnetic coupling is flexible and transmits torque through magnetic field. Therefore, it is meaningful to study the dynamic response characteristics of the magnetic coupling.

MATERIAL AND METHODS

The magnetic coupling model is shown in Figure 1 to analyze its characteristics..

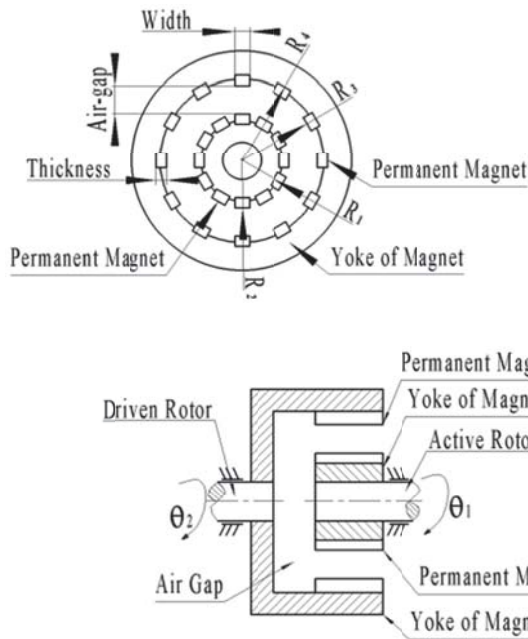


Fig. 1. Magnetic Coupling Model

The rotational inertias of the active rotor and driven rotor are J_1 and J_2 . The input torque and the output torque are T_1 and T_2 . The torsional rigidity is $k(\theta)$. The damping coefficients at the input and output sides are C_1 and C_2 . The force distribution of the magnetic coupling is shown in Figure 2. It is assumed that there is no leakage flux and the magnetic field is uniform.

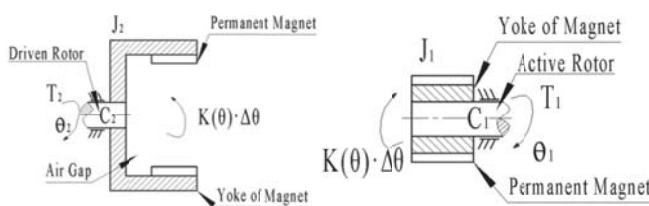


Fig. 2. Force Distribution.

According to Newton's Second Law, the following mathematical model is proposed.

$$T_1 = J_1 \ddot{\theta}_1 + C_1 \dot{\theta}_1 + k(\theta) \Delta\theta \quad (1)$$

$$k(\theta) \Delta\theta = J_2 \ddot{\theta}_2 + C_2 \dot{\theta}_2 + T_2 \quad (2)$$

$$\Delta\theta = \theta_1 - \theta_2 \quad (3)$$

When the magnetic coupling is working, the relationship between the load T_2 and the angular velocity is linear, which can be treated as a damping effect. The damping coefficient is assumed as C_d , then the following formula is obtained.

$$T_2 = C_d \dot{\theta}_2 \quad (4)$$

The torsional $k(\theta)$ rigidity changes with the angle difference $\Delta\theta$. In order to facilitate the analysis, $k(\theta)$ is assumed as a constant k . The transfer function $G_{12}(\theta)$ is defined as:

$$G_{12}(s) = \frac{\theta_2(s)}{\theta_1(s)} = \frac{k}{J_2 s^2 + C_s s + k} \quad (5)$$

where $C_s = C_2 + C_d$. From Equation (5), the driven rotor's rotating characteristic is influenced by not only the load and the torsional rigidity but also its own properties. Analyzing the influence of various parameters can help to improve the dynamic response characteristics of the driven rotor.

The synchronized characteristic between the active rotor and the driven rotor is directly affected by $\Delta\theta$. The smaller the $\Delta\theta$, the better the following performance is. Based on Equations (1)-(4), the error transfer function $G_\Delta(s)$ can be expressed as

$$G_\Delta(s) = \frac{\Delta\theta(s)}{\theta_1(s)} = \frac{J_2 s^2 + C_s s}{J_2 s^2 + C_s s + k} \quad (6)$$

According to Equation (6), $\Delta\theta$ is influenced by the rotational inertia J_2 , the damping coefficient C_s of the driven rotor and the torsional rigidity. Assuming that the magnetic coupling rotates with a constant speed a , then $\theta_1(s)$ is given by:

$$\theta_1(s) = \frac{s}{s^2} \quad (7)$$

The steady-state error e_{ss} of the magnetic coupling is described as

$$e_{ss} = \lim_{s \rightarrow 0} s E(s) = \lim_{s \rightarrow 0} s G_\Delta(s) \theta_1(s) \quad (8)$$

According to Equations (7)-(8), e_{ss} can be calculated as

$$e_{ss} = \lim_{s \rightarrow 0} s \frac{J_2 s^2 + C_s s}{J_2 s^2 + C_s s + k} \frac{s}{s^2} = \frac{a C_s}{k} \quad (9)$$

From Equation (9), the steady-state error is related to the magnetic coupling rotation speed a , the damping coefficient C_s of the driven rotor and the torsional rigidity k .

RESULTS

PROTOTYPE TEST

To choose proper parameters, prototyping experiment is taken to analyze the relationship between the torque T and the angle difference $\Delta\theta$ of the magnetic coupling. The test-bed of prototype is shown as Figure 3. The collected data is shown as Table 1. The curves of the torque T and the angle difference $\Delta\theta$ are demonstrated in Figure 4. The fourth-order equation is obtained by fitting curve, as shown in Equation (11).



Fig. 3. Test-Bed of Prototype.

Tab. 1. Collected Data between the Torque and the Angle Difference.

Type	Values									
$\Delta\theta/\text{rad}$	0	0.027	0.054	0.081	0.107	0.134	0.161	0.188	0.215	0.241
T/Nm	0	1.571	1.729	4.091	5.449	6.660	7.073	8.490	8.708	9.086
$\Delta\theta/\text{rad}$	0.268	0.295	0.322	0.349	0.376	0.403	0.429	0.456	0.483	0.523
T/Nm	9.080	8.712	8.488	7.070	6.660	5.450	4.087	1.730	1.570	0.001

The quartic fitting formula between the torque T and the angle difference $\Delta\theta$ is obtained by fitting curve as

$$T = 1052.9\Delta\theta^4 - 1056.9\Delta\theta^3 + 189.27\Delta\theta^2 + 39.312\Delta\theta - 0.06 \quad (10)$$

Hence, the torsional rigidity k is described as

$$k = 4217.6\Delta\theta^3 - 3170.7\Delta\theta^2 + 378.54\Delta\theta + 39.312 \quad (11)$$

The curve between k and $\Delta\theta$ is shown as Figure 5. The maximum torsional rigidity k is 51.72 and the initial torsional rigidity k is approximately 40.

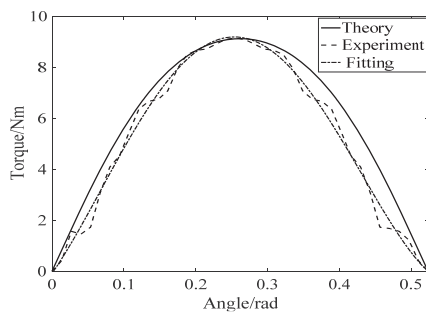


Fig. 4. Relation curve between M and $\Delta\theta$

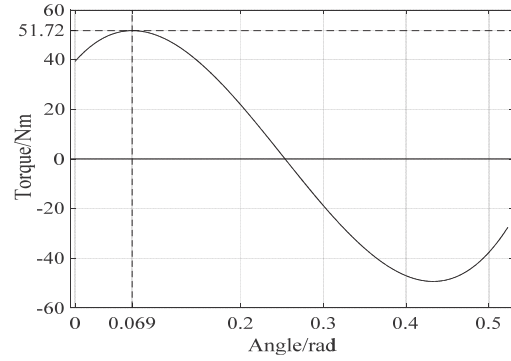


Fig. 5. Characteristic Curve between k and $\Delta\theta$.

NUMERICAL ANALYSIS

In practice, input responses are usually similar to the unit step responses which are the most detrimental, that is why we choose to analyze the unit step response characteristics of the magnetic coupling.

The Laplace transform of the step input function is written as:

$$X_1(s) = L[\varepsilon(t)] = \frac{1}{s} \quad (12)$$

The magnetic coupling output function of the unit step response is

$$X_o(s) = G_{12}(s)X_1(s) = \frac{k}{J_2s^2 + C_s s + k} \frac{1}{s} \quad (13)$$

The magnetic coupling output function in time domain is obtained from inverse Laplace transform as

$$x_o(t) = L^{-1}\left[\frac{k}{J_2s^2 + C_s s + k} \frac{1}{s}\right] \quad (14)$$

In actual engineering, the magnetic coupling will be in an unstable state when it is in over-damping or critical-damping state, resulting in the system fail. It is common to consider the under-damping state only when the magnetic coupling is designed,

In under-damping state, the magnetic coupling output function in time domain is:

$$x_o(t) = 1 - e^{-\frac{C_s}{2J_2}t} \frac{2\sqrt{J_2k}}{\sqrt{4J_2k - C_s^2}} \sin\left(\frac{\sqrt{4J_2k - C_s^2}}{2J_2}t + \arctan\left(\frac{4J_2K}{C_s\sqrt{4J_2k - C_s^2}}\right)\right) \quad (15)$$

According to the measured parameters, $C_s = 1.3716 \text{ N}\cdot\text{s} / \text{rad}$, $J_2 = 0.17 \text{ Kg}\cdot\text{m}^2$ and it is necessary that $k > 2.8 \text{ Nm} / \text{rad}$ in under-damping state. So the value of k is set as 5, 15, 30, 45, 60. The dynamic response of different torsional rigidity [19-22]. Table 2 shows the indexes of the dynamic characteristics. It can be found in Figure 6 and Table 2

that as the torsional rigidity rises, the overshoot increases, peak time and rise time decrease, however, the adjusting-time has little change. At the same time, the response oscillation becomes severe that is, the time, frequency and amplitude of oscillation increase gradually.

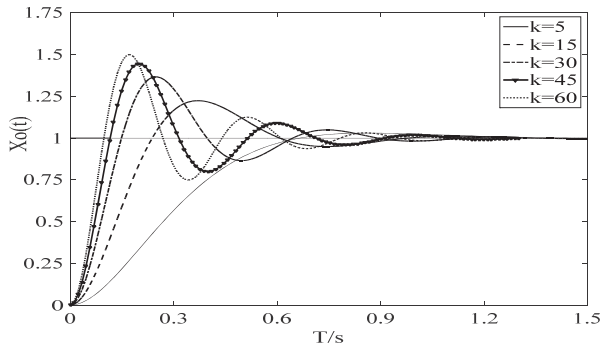


Fig. 6. The Dynamic Response Curve about k .

Tab. 2. Dynamic characteristic indexes.

Performance Indexes	Results				
Torsional Rigidity(Nm/rad)	5	15	30	45	60
Rise Time (s)	0.6649	0.2379	0.1488	0.1157	0.0975
Peak Time (s)	0.8664	0.3705	0.2483	0.1995	0.1709
Adjusting Time (s)	0.5791	0.7774	0.6045	0.6649	0.7215
Maximum Overshoot(%)	2.4283	22.1618	36.0568	44.8918	50.1817

From Figure 5, the reasonable range of the torsional rigidity k is $40 \sim 51.72 \text{ Nm/rad}$. So $k = 45 \text{ Nm/rad}$ is chosen. When $J_2 = 0.17 \text{ Kg} \cdot \text{m}^2$, the damping coefficient C_s should be less than $5.5317 \text{ N} \cdot \text{s/rad}$. Thus the value of C_s is set as 0.1, 1.5, 2.5, 3.5, 5. Figure 7 illustrates the curves of unit step dynamic response characteristics under different damping coefficients and Table 3 lists the indexes of dynamic characteristics. From Figure 7 and Table 3, with the increasing of damping coefficient C_s , the overshoot and peak time of magnetic coupling increases[23]. When the damping coefficient approaches 5.5, the magnetic coupling is closed to over-damping state, its influence on rise time is smaller and smaller with the increase of damping coefficient. when the damping coefficient is small enough, the magnetic coupling is closed to under-damping state, and the vibration tends to be persistent. Behinds, the amplitude increases with the decreasing of the damping coefficient. The smaller the damping coefficient is, the bigger the amplitude is[24].

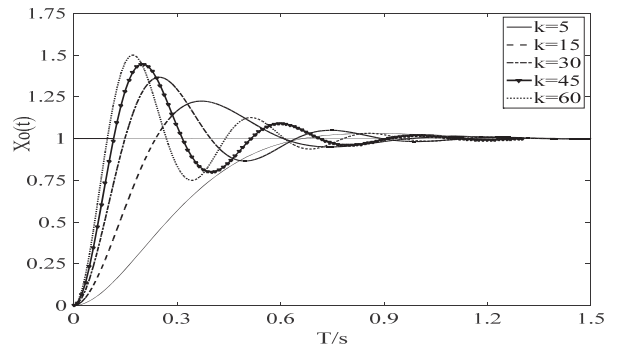


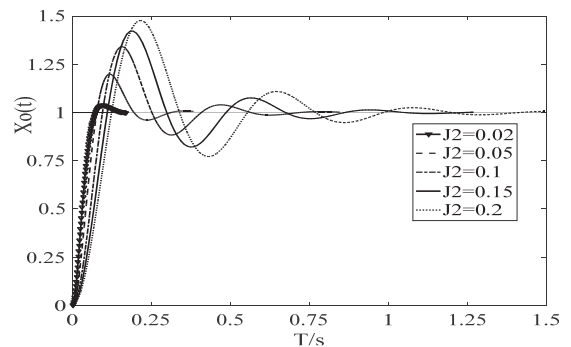
Fig. 7. Damping coefficient dynamic characteristic curves.

Tab. 3. Dynamic characteristics indexes.

Performance Indexes	Results				
Damping Coefficient	0.1	1.5	2.5	3.5	5
Rise Time (s)	0.104	0.1183	0.1410	0.1794	0.3881
Peak Time (s)	0.195	0.2009	0.2165	0.2496	0.4511
Adjusting Time(s)	10.842	0.6558	0.3231	0.3152	0.2489
Maximum Overshoot(%)	94.43	41.4261	20.3680	7.6775	0.131

According to part (1) and (2), $k = 45 \text{ Nm/rad}$, $C_s = 1.3716 \text{ N} \cdot \text{s/rad}$. The rotational inertia of the driven rotor should satisfy $J_2 > 0.0105 \text{ Kg} \cdot \text{m}^2$. The value of J_2 is set as 0.02, 0.05, 0.1, 0.15, 0.2. Figure 8 shows the curves of unit step dynamic response characteristics. Table 4 shows the indexes. From Figure 8 and Table 4, with the increase of rotational inertia, the rise time, the overshoot, the peak time and the adjusting time of the magnetic coupling rises, while the acceleration of the driven rotor reduces.

Fig. 8. The Curves of Dynamic Characteristics about Rotational Inertia.



Tab. 4. Dynamic characteristics index.

Performance index	Result				
	0.02	0.05	0.1	0.15	0.2
Rotational inertia	0.02	0.05	0.1	0.15	0.2
Rise time (s)	0.0728	0.0767	0.0949	0.1105	0.1235
Peak time (s)	0.0955	0.1176	0.1566	0.1878	0.2151
Accommodation time (s)	0.0637	0.1755	0.375	0.6149	0.7364
Maximum time (%)	3.7369	19.8887	34.2038	41.9949	49.5937

DISCUSSION

Based on the analysis mentioned above, the dynamic characteristics of the magnetic coupling are impacted by the torsional rigidity k , the damping coefficient C_s and the rotational inertia J_2 of the driven rotor. Once the magnetic coupling has been installed, the rotational inertia J_2 and the damping coefficient C_s are fixed. However, the torsional rigidity k and the dynamic characteristics varies with the changes of angle difference $\Delta\theta$. To realize the required dynamic performance of the magnetic coupling, the reasonable range of the torsional rigidity k should be defined and the operating angle is supposed to ensure this range. If it is hard to meet the requirements in design, the external contributor can be applied to change the rotational inertia J_2 and the damping coefficient C_s .

CONCLUSIONS

It is obvious that the torsional rigidity k , the damping coefficient C_s and the rotational inertia J_2 have different effects on the dynamic characteristics of the magnetic coupling.

According to the steady-state error, the steady performance is closely associated with the torsional rigidity k and the damping coefficient C_s . But it is not effected by the rotational inertia J_2 which only has influence on the startup process of the magnetic coupling.

A large rotational rigidity k contributes to steady characteristics, startup characteristics and response characteristics, yet it leads to large overshoot and severe fluctuation. A small damping coefficient C_s will improve the steady performance of the magnetic coupling but it will result in serious oscillation. A large damping coefficient will cause the over-damping state and reduce the stability of magnetic coupling. The rotational inertia J_2 has no effects on steady characteristics of the magnetic coupling. But it affects the startup stage. Though the small rotational inertia has benefit to the startup characteristic, it makes the magnetic coupling approach over-damping state. Therefore, the reasonable torsional rigidity and damping coefficient

should be chosen, and the rotational inertia should be neither too large nor too small.

ACKNOWLEDGEMENTS

The research is supported by the Fundamental Research Funds of Shandong University (Project no.2016JC035) and the Natural Science Foundation of Shandong Province (Project no.ZR2016WH02), which are gratefully acknowledged.

REFERENCES

1. Zheng, C.W. and C.Y. Li, "Variation of the wave energy and significant wave height in the China Sea and adjacent waters", *Renewable and Sustainable Energy Reviews*, 43, 381-387, 2015.
2. Wu, S., C. Liu, and X. Chen, "Offshore wave energy resource assessment in the East China Sea", *Renewable Energy*, 76, 628-636, 2015.
3. Rute Bento, A., P. Martinho, and C. Guedes Soares, "Numerical modelling of the wave energy in Galway Bay", *Renewable Energy*, 78: p. 457-466, 2015.
4. Parkinson, S.C., et al., "Integrating ocean wave energy at large-scales: A study of the US Pacific Northwest", *Renewable Energy*, 76: p. 551-559, 2015.
5. Behrens, S., et al., "Wave energy for Australia's National Electricity Market", *Renewable Energy*, 81: p. 685-693, 2015.
6. Astariz, S. and G. Iglesias, "The economics of wave energy: A review", *Renewable and Sustainable Energy Reviews*, 45: p. 397-408, 2015.
7. Wang, Y.-L., "A wave energy converter with magnetic gear", *Ocean Engineering*, 101: p. 101-108, 2015.
8. Siegel, S.G., 2015. Wave radiation of a cycloidal wave energy converter", *Applied Ocean Research*, 49: p. 9-19, 2015.
9. Cordonnier, J., et al., "SEAREV: Case study of the development of a wave energy converter", *Renewable Energy*, 80: p. 40-52, 2015.
10. Tiron, R., et al., "The challenging life of wave energy devices at sea: A few points to consider", *Renewable and Sustainable Energy Reviews*, 43: p. 1263-1272, 2015.
11. de Andres, A., et al., "Adaptability of a generic wave energy converter to different climate conditions", *Renewable Energy*, 78: p. 322-333, 2015.

12. Bacelli, G. and J.V. Ringwood, "Numerical Optimal Control of Wave Energy Converters", *Sustainable Energy*, 2(6): p. 294-302, 2015.
13. Krasilnikov, A.Y. and A.A. Krasilnikov, "Influence of type of high-coercivity permanent magnet on characteristics of end magnetic clutch", *Chemical and Petroleum Engineering*, 47(3): p. 186-192, 2011.
14. Staff, "Magnetic coupling protects machinery", UBM Canon LLC: Manhasset. p. 26, 1999,
15. Uno, "M., et al., Development of the Floating Centrifugal Pump by Use of Non Contact Magnetic Drive and Its Performance", *International Journal of Rotating Machinery*, 10(5): p. 337-344, 2004.
16. Krasilnikov, A.Y. and A.A. Krasilnikov, "Magnetic clutches and magnetic systems in sealed machines", *Chemical and Petroleum Engineering*, 48(5): p. 306-310, 2012.
17. Krasilnikov, A.Y., "Order of Selection and Design of Magnetic Clutches for Sealed Machines", *Chemical and Petroleum Engineering*, 49(7): p. 467-475, 2013.
18. Zhu, Z. and Z. Meng, "3D analysis of eddy current loss in the permanent magnet coupling", *Review of Scientific Instruments*, 87(7): p. 074701, 2016.
19. Isemael, Y.Y. "Molecular, Histological and biochemical effects of tea seed cake on hepatic and renal functions of *Oreochromis niloticus*", *Acta Scientifica Malaysia*, 1(1): p. 13-15, 2017.
20. Soehady, H.F. Asis, J. Tahir, S. Musta, B. Abdullah, M. Pungut, H. "Geosite Heritage and Formation Evolution of Maga Waterfall, Long Pasia, South of Sipitang, Sabah", *Geological Behavior*, 1(2): p. 34-38, 2017.
21. Ismail, I. Husain, M.L. Zakaria, R. "Attenuation of Waves From Boat Wakes In Mixed Mangrove Forest Of *Rhizophora* And *Bruguiera* Species In Matang, Perak", *Malaysian Journal Geosciences*, 1(2): p. 32-35, 2017.
22. Radmanfar, R.Rezayi, M. Salajegheh, S. Bafrani, V.A. "Determination the most important of hse climate assessment indicators case study: hse climate assessment of combined cycle power plant staffs", *Journal CleanWAS*, 1(2): p. 23-26, 2017.
23. Yasin, H. Usman, M. Rashid, H. Nasir, A. Sarwar, A. Randhawa, I.A. "Guidelines for Environmental Impact Assessment of JHAL flyover and underpass project in Faisalabad", *Geology, Ecology, and Landscapes*, 1(3): p. 205-212, 2017.
24. Hassan, M.A. Ismail, M.A.M. "Literature Review for The Development of Dikes's Breach Channel Mechanism Caused by Erosion Processes During Overtopping Failure", *Engineering Heritage Journal*, 1(2): p. 23-30, 2017.

CONTACT WITH THE AUTHOR

Yanjun Liu

e-mail: lyj111ky@163.com

School of Mechanical Engineering
Shandong University
Jinan, Shandong 250061
CHINA